

Communication

Tightly Embedded Modular Antenna-in-Display (MAiD) Into the Panel Edge of Display With Dual-Polarization for 5G Smartphones

Jeongtaek Oh, Kiseo Kim, Jaek Choi, and Jungsuek Oh 

Abstract—This study introduces a novel modular antenna-in-display (MAiD) concept for advanced smartphone antenna modularization. It focuses on dual-polarization integration in a compact space within the display panel, essential for millimeter-wave (mmWave) 5G smartphones operating in the n257 and n258 bands of FR2. The adaptable MAiD is compatible with various displays, including foldable and slidable types. The MAiD ingeniously utilizes the display panel's dead space (DS), a narrow 300- μm area, for antenna placement. This innovation is integrated into the same layer as the touch sensor (TS). We propose two 1×4 antenna array configurations within the DS for dual-linear polarization, enhancing capacity through selection diversity. The antennas, named antenna-in-display parallel to DS (AiD-pDS) and antenna-in-display normal to DS (AiD-nDS), are fabricated with a 50- μm -thick polyimide film. Their design allows embedding in a $0.03\lambda_0$ width of the DS. The MAiD achieves impressive 10-dB return-loss bandwidths of 26.7–28.6 GHz and 24.5–28.1 GHz, with measured boresight gains of 9.041 and 8.824 dBi for AiD-pDS and AiD-nDS, respectively. It maintains over 12-dB cross-polarization level (XPL), demonstrating its effectiveness for modern smartphone technologies.

Index Terms—5G smartphone, antenna-in-display (AiD), display-integrated antenna, millimeter wave (mmWave), module-embedded antenna.

I. INTRODUCTION

As the next-generation 5G network evolves, it demands significantly improved performance, including broader beam coverage and higher radiation efficiency for mobile communication systems. This advancement presents new technical challenges for the modular design of antennas. Specifically, for millimeter-wave (mmWave) antennas, there are key objectives: 1) increasing radiation efficiency while minimizing loss in the fabrication process, which requires finer and higher resolutions; 2) enhancing selection diversity through multiple polarizations; and 3) developing antenna designs that integrate with adjacent structures in a novel packaging concept.

Antenna-in-package (AiP) technology has emerged as a leading solution for various mmWave applications. It incorporates multiple techniques to optimize RF performance, such as compact size, wide and multiband bandwidth, and high gain [1], [2], [3], [4], [5], [6], [7], [8], [9], [10]. Notably, the implementation of stacked patch-type antennas in multiple substrates has led to the development of dual-polarized AiP designs. However, AiP technologies face practical

challenges of performance variations when antennas are combined with different materials, such as a rear glass case [1], [2], [3]. Efforts to mitigate radiation loss effects and integrate antennas with surrounding metasurfaces beneath the rear glass cover have shown promise, but further research in low profile and complementary stack-up in the bezel area is still needed [4].

The antenna-in-display (AiD) technology and the antenna-on-display (AoD) technology introduce a novel concept of integrating antennas within the display, aiming to provide beam coverage in the front glass direction of smartphones [11], [12], [13]. The AiD configuration is comprised of a multilayered structure, including the front cover glass, optically clear adhesives (OCAs), polarizers, and display panels equipped with conductive electrodes. Expanding on this foundation, the modular AiD (MAiD) concept is first suggested. The MAiD integrates a super-thin antenna module directly into the display panel, heralding a novel antenna-integrated display panel for future smartphone features. This approach is distinct from the AoD technology, as MAiD streamlines the design by removing the need for additional transparent antenna films. Instead, the antenna radiator is ingeniously integrated into the touch sensor panel (TSP) layer, where it exists in harmony with the touch sensor (TS) electrodes. A critical aspect of the MAiD is the strategic use of the display panel's dead space (DS). The radiating trace's area is meticulously confined to the DS, specifically defined as $0.03\lambda_0$ at 28 GHz. This limitation is intentional to ensure that MAiD does not encroach upon the active area (AA) of the display, which is reserved for other essential electrodes. By adhering to these parameters, MAiD achieves a balance between advanced functionality and the integrity of the display.

For future 5G cellular communications, the use of dual-polarized antenna arrays is increasingly vital due to the random orientations of mobile terminals relative to base stations [6], [10], [14], [15], [16], [17]. However, manufacturing such antennas faces constraints, particularly in the limited space available at the edge of devices, necessitating a minimum width of 0.25λ , considering monopole or dipole geometry. In the case of the AoD, this width requirement inevitably infringes upon the AA of the display, making it challenging to apply to commercial products [11]. In contrast, the MAiD not only reduces fabrication costs by eliminating the need for additional film but also operates with dual-polarization without encroaching on the AA of the display, which provides a significant commercial advantage. To address this, dual-polarization and impedance matching techniques for uniplanar antennas are being explored [5], [14], [18], [19], [20], [21], [22].

In this communication, the MAiD is proposed with two geometries to support dual-linear polarization. In [12], the AiD concept was suggested and demonstrated in mmWave spectrum, and it was single linear-polarized. The available polarization in the single layer of the DS can be defined based on the edge of the DS. The first proposed AiD is polarized in parallel with the DS (AiD-pDS), with a more miniaturized dimension compared to the antenna size of [12]. The

Received 19 July 2024; revised 3 November 2024; accepted 13 November 2024. Date of publication 25 November 2024; date of current version 5 February 2025. This work was supported in part by Samsung Display Company Ltd. and in part by the Institute of Information and Communications Technology Planning and Evaluation (IITP) Grant funded by Korean Government (MSIT) (Millimeter-Wave Metasurface-Based Dual-Band Beamforming Antenna-on-Package Technology for 5G Smartphone) under Grant 2020-0-00858-004. (Corresponding author: Jungsuek Oh.)

Jeongtaek Oh and Jungsuek Oh are with the Department of Electrical and Computer Engineering, Institute of New Media and Communications (INMC), Seoul National University, Seoul 08826, South Korea (e-mail: iwalife@snu.ac.kr; jungsuek@snu.ac.kr).

Kiseo Kim and Jaek Choi are with Samsung Display Company Ltd., Kiheung 17113, South Korea.

Digital Object Identifier 10.1109/TAP.2024.3501415

0018-926X © 2024 IEEE. Personal use is permitted, but republication/redistribution requires IEEE permission.

See <https://www.ieee.org/publications/rights/index.html> for more information.

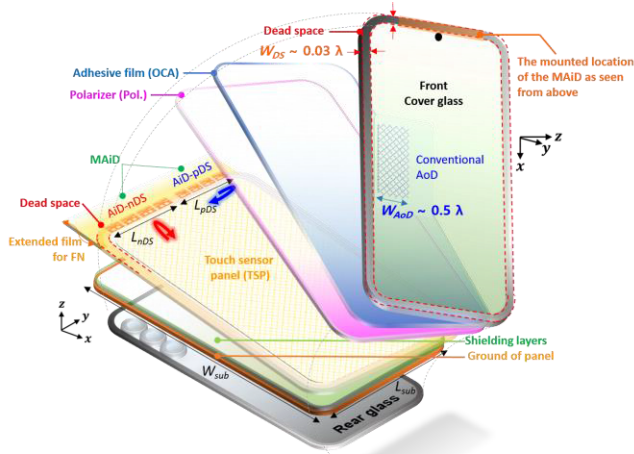


Fig. 1. Tear-down stack-up of the display panel of a smartphone and the proposed dual-polarized MAiD array configurations compared to the conventional AoD.

second AiD polarized in normal with the DS (AiD-nDS) is proposed with symmetrical geometry to radiate with a polarization normal to the edge of the DS. The proposed MAiD was fabricated by departing substrate by the radiating trace and the substrate of a feeding network, to conform to the merchandizing process of a display panel.

II. AiD ELEMENT DESIGN

Fig. 1 illustrates the schematic of the proposed dual-linear-polarized MAiD array, alongside the stack-up of the multilayered display structure. This figure demonstrates the alignment of dual-linear-polarized antennas, arranged in two distinct 1×4 subarrays along the edge of the DS. The AoD antenna is also depicted in Fig. 1 for a size comparison with the MAiD. Notably, the MAiD significantly reduces the intrusion into the AA, achieving a design, that is, approximately 16.7 times smaller than the AoD, at the same time ensuring no interference with display visibility. The substrate dimensions were 70.9×146.3 mm ($L_{sub} \times W_{sub}$), corresponding to the size of a commercial smartphone screen. The display structure consists of several layers, both above and below the display panel, meticulously arranged to create the final product. The detailed dimensions of the materials used in the stack-up are provided in Table I. The radiators are printed on the same layer of the TSP layer, where the proposed MAiD was optimized in $300 \mu\text{m}$ width of the DS. In addition, there is a gap between the antenna pattern and the TS electrodes as shown in Fig. 2(a) and (b). The optimized dimensions of AiD-pDS and AiD-nDS are listed in Table II. The AiD-pDS radiator is designed as an asymmetrical folded dipole antenna (FDA), inductively fed by a coplanar waveguide. In contrast, the AiD-nDS radiator employs a symmetrical slot dipole antenna (SSDA), which is capacitively fed by a coplanar waveguide.

A. AiD-pDS Topology

An asymmetrical FDA with a slit-ended edge of the dipole is chosen as the radiator of the AiD-pDS as shown in Fig. 2(a). The asymmetrical FDA for the AiD application was verified in [12]; however, the slits at the edge of the dipole are suggested for an enhancement of the impedance matching. The slit structure at the edge of the FDA is employed as a reactive loading scheme. The FDA is optimized with a length (L_{a6}) of 0.658λ at 28 GHz, and

TABLE I

SUMMARY OF SUBSTRATE THICKNESS FROM THE TOP OF THE FIRST LAYER FACING THE FRONT-SIDE DIRECTION (UNIT: WAVELENGTH)

Layer	Name	Thickness	Relative permittivity (ϵ_r)
1	Cover glass	0.0448	6.9
2	OCA	0.014	2.57
3	Pol.	0.0097	2.92
4	PI under TSP	0.0047	3.3
5	Shielding layers	0.0152	2.62

The thickness is expressed in units of wavelength at 28 GHz. The relative permittivity was provided from Samsung display company, and estimated at 10 GHz.

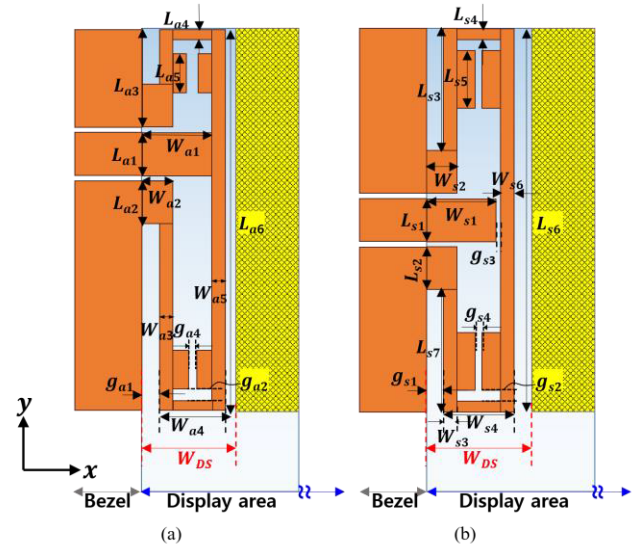


Fig. 2. (a) Single element geometry of AiD-pDS. (b) Single element geometry of AiD-nDS.

TABLE II

OPTIMIZED DIMENSIONS OF THE SINGLE ANTENNA IN FIG. 2 (UNIT: WAVELENGTH)

Design parameter	Fig. 2 (a)	Design parameter	Fig. 2 (b)
L_{a1}	0.020	L_{s1}	0.085
L_{a2}	0.17	L_{s2}	0.076
L_{a3}	0.093	$L_{s3} (= L_{s7})$	0.085
L_{a4}	0.008	L_{s4}	0.0085
L_{a5}	0.034	L_{s5}	0.025
L_{a6}	0.658	L_{s6}	0.423
W_{a1}	0.042	W_{s1}	0.037
W_{a2}	0.011	W_{s2}	0.01
W_{a3}	0.007	W_{s3}	0.005
W_{a4}	0.028	W_{s4}	0.042
W_{a5}	0.007	W_{s5}	0.008
g_{a1}	0.004	W_{s6}	0.005
g_{a2}	0.007	g_{s1}	0.005
g_{a4}	0.003	g_{s3}	0.006
		g_{s4}	0.003

The thickness is expressed in units of wavelength at 28 GHz.

the return loss is shown to compare impedance matching with and without the slit structure in Fig. 3(a). The feeding method of the AiD-pDS is well matched by the inductively fed CPW line as shown in Fig. 4(a), and the design parameter of asymmetrical degree (L_{a3}) is optimized based on the observation that the input impedance of the

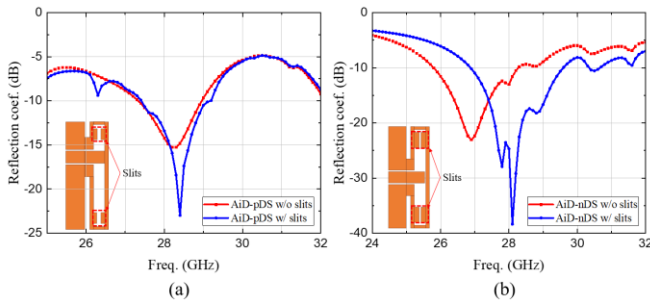


Fig. 3. Reflection coefficient along frequency to compare (a) AiD-pDS with and without slits and (b) AiD-nDS with and without slits.

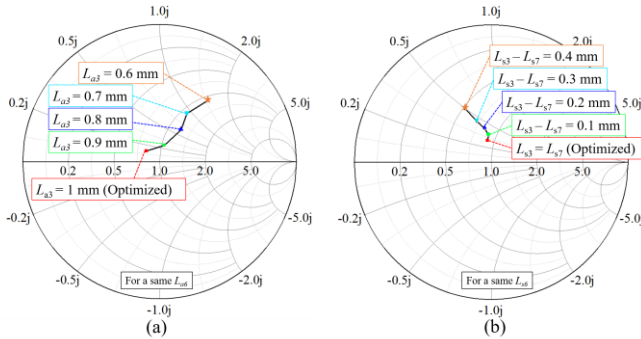


Fig. 4. Smith chart of (a) AiD-pDS and (b) AiD-nDS to compare the characteristics of impedance matching along the feeding point.

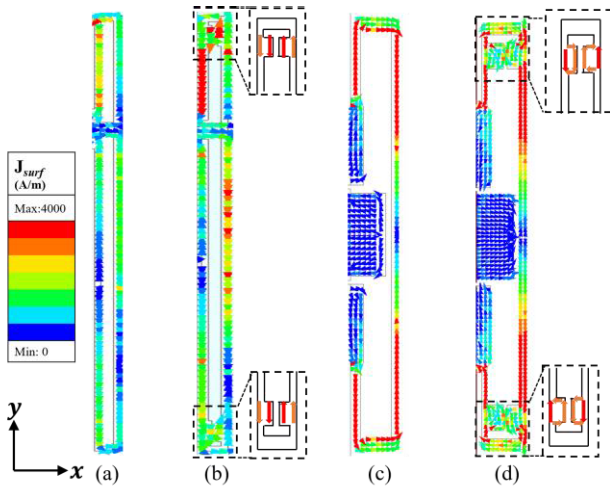


Fig. 5. Simulated surface current vector distribution of (a) AiD-pDS with slits, (b) without slits, (c) AiD-nDS with slits, and (d) without slits.

dipole is lower at the edges compared to the center. The orientation of polarization is dictated by the asymmetrical geometry inherent in the AiD-pDS. This is primarily attributed to the distribution of peak current vectors, which serves as the reason. The surface current vector distribution of the AiD-pDS without and with the slit structure is shown in Fig. 5(a) and (b), respectively, which shows that the current path is inductively changed by the slit. The radiation pattern of a single AiD-pDS is shown in Fig. 6(a). The 10-dB return-loss bandwidth of the proposed AiD-pDS is 27.41–29.17 GHz, and the peak realized gain is 3.56 dBi at 28 GHz.

B. AiD-nDS Topology

The radiator of the AiD-nDS is intended to radiate with orthogonal polarization from the AiD-pDS, which must be normal to the width direction of the DS. The AiD-nDS is an SSSA with a slit-ended edge

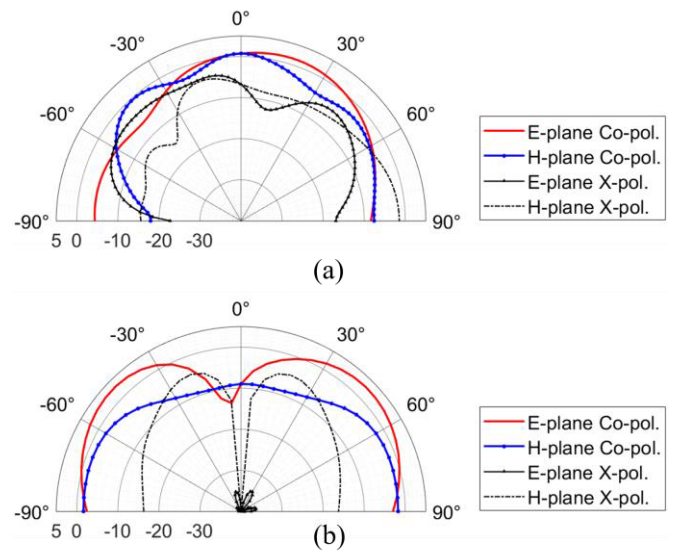


Fig. 6. Far-field radiation pattern of single element antenna at 28 GHz. (a) AiD-pDS and (b) AiD-nDS.

of the dipole as shown in Fig. 2(b). The slit structure at the edge of the SSSA is employed for better impedance matching, and wider bandwidth by dual-resonant frequency as shown in Fig. 3(b). The proposed SSSA is capacitively fed by the CPW line with a gap (g_3), based on the observation that the input impedance of the center of the dipole is higher compared to an asymmetric offset as illustrated in Fig. 4(b). The symmetrical dipole with a slit structure is beneficial for miniaturization and high cross-polarization level (XPL) [15]. In Fig. 5(c) and (d), the current vector distribution goes in opposite directions around the center of the signal line. The extra current path by the slit structure in the AiD-nDS in Fig. 5(d) corresponds to the dual-resonant frequency in Fig. 3(b). The radiation pattern of a single AiD-nDS is shown in Fig. 6(b), and the XPL of all directions in the E-plane (XoZ plane) is lower than 30 dB because the current vector distribution parallel to the DS is canceled from the symmetric geometry. The 10-dB return-loss bandwidth of the single AiD-nDS is 25.79–28.28 GHz, and the peak realized gain is 3.1 dBi at 28 GHz.

III. ARRAY FOR DUAL-LINEAR-POLARIZED AiD

The proposed AiD-pDS and AiD-nDS arrays, each consisting of 1×4 elements, have been fabricated to verify the performance of beam synthesis. Fig. 7 illustrates the feeding network, which comprises two distinct feeding structures. The radiators of these antenna arrays were patterned on a $50\text{-}\mu\text{m}$ -thick PI film. The coplanar waveguide feed lines are patterned with a 1.5 mm width for anisotropic conductive film (ACF) bonding. The interelement period of the array is 0.51λ at 28 GHz. Each feed structure is designed with a specific purpose.

A. Feeding Network #1 (FN #1)

This utilizes a plug-type RF connector suitable for commercial applications. The feed lines of the arrays are electrically connected with FN #1 via ACF bonding. Each antenna element is connected to an individual port on the header of the plug connector through grounded coplanar waveguide transmission lines. The substrate of FN #1 is a flexible PCB, 50 μm in thickness and with a relative permittivity of 3.5. The dimensions of FN #1 are 29×15 mm.

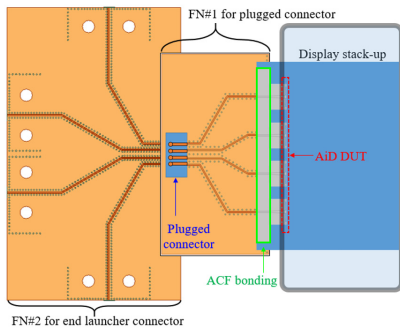


Fig. 7. Configuration of an array sample for the proposed AiD DUT.

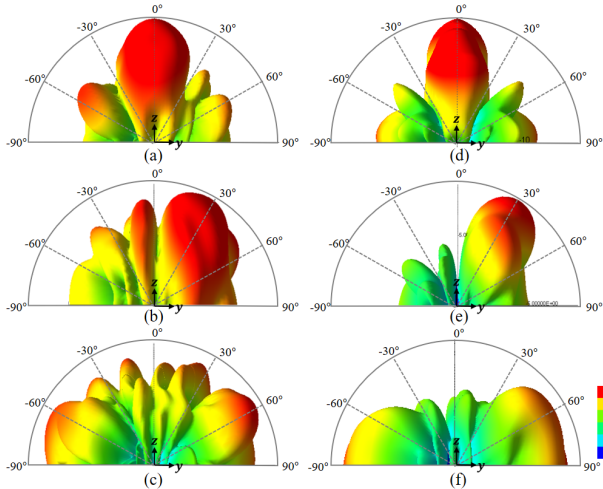


Fig. 8. Simulated 3-D patterns of beam steering for (a) boresight, (b) 30° tilt, (c) 60° tilt of the AiD-pDS array, (d) boresight, (e) 30° tilt, and (f) 60° tilt of the AiD-nDS array.

B. Feeding Network #2 (FN #2)

This network is designed for the actual measurement of antenna samples, utilizing end launcher connectors. Transmission lines of equal length are connected to each port of plug connectors to the end launcher ports. FN #2 is fabricated using the same type of flexible PCB as FN #1. The dimensions of FN #2 are 42.5×25 mm.

The radiation characteristics of the proposed AiDs, were verified for beam-tilting performance, including the feeding network in Fig. 7. The far-field beam-tilting characteristics of the proposed AiD arrays are shown in Fig. 8. In Fig. 8(c) and (f), it can be observed that the main lobe is tilted by 60° for the AiD-pDS and AiD-nDS, respectively.

IV. INTEGRATED AiD FABRICATION AND EVALUATION

Based on the proposed antennas for dual-linear polarization, the 1×4 linear antenna arrays for each polarization type are designed for verification of beam synthesized gain in a quad-channel beam forming system. The radiators of the proposed AiDs are fabricated by photolithography process on the PI film and affixed to the display panel as shown in Fig. 9(a). The antenna is covered by a front glass. Fig. 9(b) and (c) shows the micrographs of the AiD-pDS array and AiD-nDS array bonded to FN #1 before it is embedded in the display panel. The return-loss characteristics of the fabricated antenna arrays were measured using a vector network analyzer (VNA). The return loss for each port in the antenna array is measured by terminating the other port to 50Ω . The measured -10 -dB reflection coefficient data

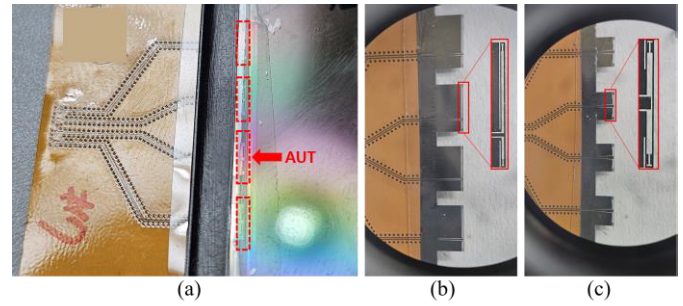


Fig. 9. (a) Fabricated antenna array embedded in the display panel and FN #1. Micrographs of (b) AiD-pDS array and (c) AiD-nDS array.

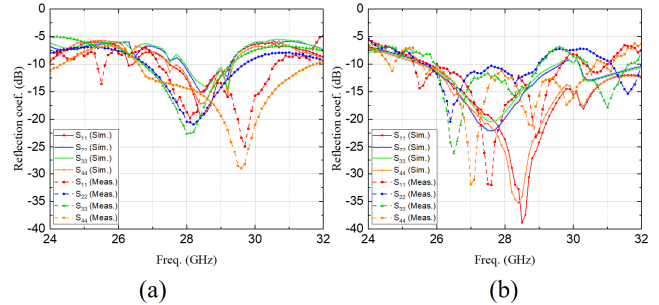


Fig. 10. Comparison of simulated active S-parameter and measured reflection coefficient for (a) AiD-pDS and (b) AiD-nDS.

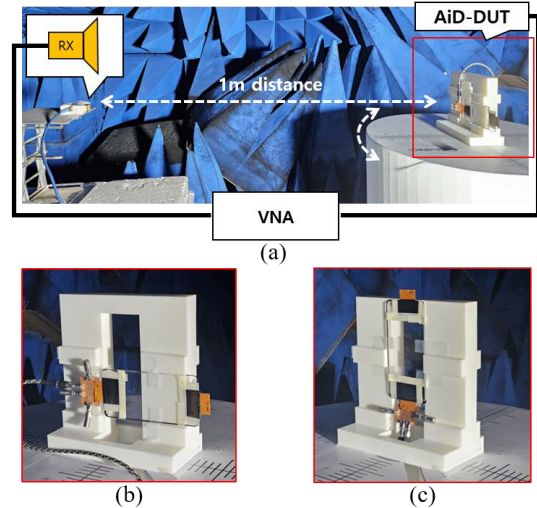


Fig. 11. (a) Measurement setup with a signal generator, and DUT setup on (b) E-plane, and (c) H-plane.

are compared with the simulated active S-parameter in Fig. 10. The measured -10 -dB return-loss bandwidth was 26.7–29.3 GHz for the AiD-pDS in Fig. 10(a). This bandwidth value is based on the inside ports, although the bandwidth based on outside ports is wider than the one with inside ports, because of an additional resonant frequency at 29.5 GHz caused by a fabrication error. In the case of the AiD-nDS, the resonant frequency is divided around 28 GHz, and the measured bandwidth of the AiD-nDS is 25.7–28.6 GHz as shown in Fig. 10(b). The transmission line loss of FN #2 is measured as 0.069 dB/mm at the target bandwidth.

The far-field radiation patterns of the fabricated antennas were measured in an mmWave anechoic chamber at Seoul National University, Seoul, South Korea, and the experimental measurement setup

TABLE III
COMPARISON WITH STATE-OF-THE-ART mmWave ANTENNAS EMPLOYING DISPLAY

Ref.	This work	[6]	[11]	[12]	[14]
Topology	Asymmetrical folded dipole/ Symmetrical slot dipole	Monopole/ dipole	Differentially-fed patch	Asymmetrical folded dipole	Dipole/Slot dipole
Type of Metallic layer	Al-alloy	Copper	Diamond-grid Ag-alloy	Copper	Copper
Substrates	50 μm PI	55–60 μm Multiple Ceramic layers	40 μm COP	50 μm COP	1.575 mm Rogers 5870
Array Size	Two 1×4 subarrays	1×4	1×4	1×4	Two 1×8 Subarrays
Peak Array Antenna Gain (dBi)	9.041/8.829	9.2/8	9.45/9.50 (at 28 GHz) 8.99/8.14 (at 39GHz)	12.32	4–7.5 (26.5–90 GHz)
Max. Rad. Eff (%)	78.7/88.6	80/85	N.A.	54.3	60–90
Process	Photolithography	LTCC	Photolithography	Photolithography	Single-layer PCB
Polarization	Dual linear	Dual linear (H/V)	Dual linear (Switchable)	Single linear	Dual linear
-10 dB Bandwidth (GHz)	27.3–29.3 (7%)/ 25.7–28.6(10%), Meas.)	26.6–36/ 27.35– 31.1 (Meas.)	26.2–38.1 (37%, Simul.)	25.3–31.2 (30.3%, Meas.)	24.4–46.4 (100%) * -6 dB reference
Cross Polarization Level (dB)	14.4/22.5	25	20	N.A.	5
Beam Steering($^\circ$)	0–60/0–30	0–30	-35–35	0–60	0–75

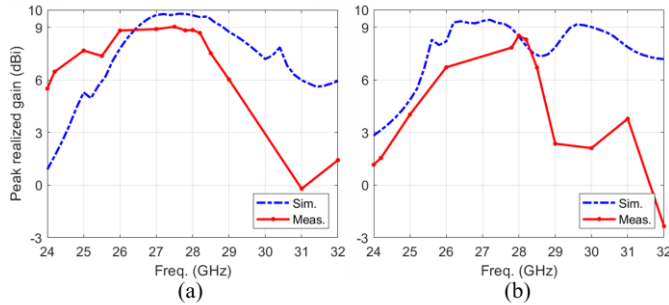


Fig. 12. Measured and simulated gains of (a) AiD-pDS and (b) AiD-nDS along the operation band.

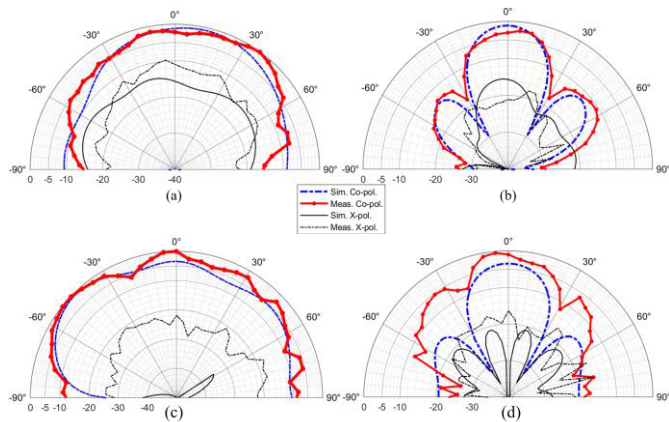


Fig. 13. Measured and simulated results of the normalized radiation pattern of the 1×4 AiD-pDS array prototype on (a) E-plane and (b) H-plane, and the 1×4 AiD-nDS array prototype on (c) E-plane and (d) H-plane at 28 GHz.

is shown in Fig. 11(a). The revolving arm with the antenna under test (AUT) was rotated in the hemisphere range, and the gain was

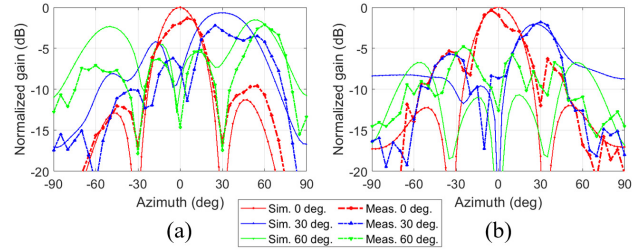


Fig. 14. Measured and simulated plot of the normalized scanned far-field patterns of the fabricated cellular prototype featuring dual-polarized MAiD. (a) AiD-pDS (X -axis polarization) and (b) AiD-nDS (Y -axis polarization).

measured by a standard gain horn (A-INFO 22–32). A 3-D-printed zig is fabricated to fix the smartphone glass on the E-plane in Fig. 11(b) and on the H-plane in Fig. 11(c).

Fig. 12 illustrates the gain of the fabricated 1×4 antenna arrays. The AiD-pDS array is measured with a maximum gain of 9.041 dBi at 27.5 GHz, and the measured 3-dB gain–bandwidth covers 24.2–29 GHz, approximately shifted by 2 GHz from simulated gain–bandwidth as shown in Fig. 12(a). The AiD-nDS array is measured with a maximum gain of 8.829 dBi at 28 GHz, and the measured 3-dB gain–bandwidth covers 25.7–28.5 GHz, in good agreement with to lower band of simulated gain–bandwidth as shown in Fig. 12(b). The measurement range of the E-plane (XoZ plane) and H-plane (YoZ plane) corresponds to the range of the hemisphere where the normal to the display (Z -axis) is assumed to be 0° . The measured and simulated normalized radiation patterns of the fabricated prototype of the proposed antenna array are shown in Fig. 13. The co-polarized direction of the AiD-pDS is parallel to the DS (X -axis direction). The peak gain of the AiD-pDS is measured at $\theta = 30^\circ$ on the E-plane at 27.5 GHz, and the HPBW is 60.9° (-17.7° to 53.2°) as shown in Fig. 13(a). The measured XPL of the AiD-pDS at the boresight is 14.4 dB. The co-polarized direction of

the AiD-nDS is normal to the DS (Y -axis direction) in Fig. 13(c) and (d). The peak gain of the AiD-nDS is measured at $\theta = 0^\circ$ on the E-plane at 28 GHz. The HPBW of the AiD-nDS on the E-plane is 36.01° (-65.16° to -29.15°), and the XPL of the AiD-nDS at the boresight is 22.5 dB with the simulated boresight at $\theta = -60^\circ$ as a reference angle. The boresight angle as a reference is determined by the simulation, because the peak gain at $\theta = 0^\circ$ on the E-plane was unexpected, and the radiation pattern from the rest of the angle followed the simulated radiation pattern. The measured XPL of the AiD-nDS at the boresight is 22.4 dB. The scanning ability of the fabricated prototypes was tested using the AEP technique. The beam tilting was calculated by a phase difference of each port multiplied by the measured element factor for each port of the array, and the beam scanning results are shown in Fig. 14. The scanning ability of the AiD-pDS (X -axis polarization) is 60° in Fig. 14(a), and the scanning ability of the AiD-nDS (Y -axis polarization) is 30° with 3-dB scan loss in Fig. 14(b). The performance comparison of this work and some state-of-the-art antennas is summarized in Table III.

V. CONCLUSION

For the first time, a novel modularization architecture of MAiD and 1-D AiD array is proposed with dual-linear polarization and good XPL. The proposed dual-polarized MAiD enables to receive orthogonal polarization signals from two different subarrays of the AiD-nDS and the AiD-pDS at the 28-GHz band and provides sufficient properties in terms of impedance matching, gain, and beam coverage. Ultimately, dual-linear polarization is realized with a satisfying compact size in $0.03\lambda_0$ at 28 GHz of the DS at the same time. The proposed MAiD in the DS of a display panel leads to the novel mounting space of the antenna package, accompanied by compatibility with novel displays for 5G mobile smartphones, such as foldable and slidable displays.

REFERENCES

- [1] C. Ju Park, D. Jung, J. Seo, T. Sun Kwon, B. Ahn, and S.-H. Wi, "Isolation improvement technique in dual-polarized antenna for sub-THz antenna-in-package," *IEEE Antennas Wireless Propag. Lett.*, vol. 22, pp. 3032–3036, 2023.
- [2] Y. Zhang and J. Mao, "An overview of the development of antenna-in-package technology for highly integrated wireless devices," *Proc. IEEE*, vol. 107, no. 11, pp. 2265–2280, Nov. 2019.
- [3] J. Seo et al., "Miniaturized dual-band broadside/endfire antenna-in-package for 5G smartphone," *IEEE Trans. Antennas Propag.*, vol. 69, no. 12, pp. 8100–8114, Dec. 2021.
- [4] J. Jung, W. Lee, G. Lee, S. Hong, and J. Oh, "Ultra-thinned metasurface-embedded smartphone antenna-in-package for millimeter-wave 5G/6G coverage enhancement," *IEEE Trans. Antennas Propag.*, vol. 71, no. 10, pp. 7766–7781, Oct. 2023.
- [5] R. Hussain and M. S. Sharawi, "An integrated slot-based frequency-agile and UWB multifunction MIMO antenna system," *IEEE Antennas Wireless Propag. Lett.*, vol. 18, no. 10, pp. 2150–2154, Oct. 2019.
- [6] H.-T. Chou, S.-J. Chou, J. D. S. Deng, C.-H. Chang, and Z.-D. Yan, "LTCC-based antenna-in-package array for 5G user equipment with dual-polarized endfire radiations at millimeter-wave frequencies," *IEEE Trans. Antennas Propag.*, vol. 70, no. 4, pp. 3076–3081, Apr. 2022.
- [7] T. H. Lin et al., "Broadband and miniaturized antenna-in-package (AiP) design for 5G applications," *IEEE Antennas Wireless Propag. Lett.*, vol. 19, no. 11, pp. 1963–1967, May 2020.
- [8] J. Park, D. Choi, and W. Hong, "Millimeter-wave phased-array antenna-in-package (AiP) using stamped metal process for enhanced heat dissipation," *IEEE Antennas Wireless Propag. Lett.*, vol. 18, no. 11, pp. 2355–2359, Nov. 2019.
- [9] J. Jung and J. Oh, "3D tempered glass-covered metasurface antenna-in-package enabling reliable 5G/6G smartphone beam coverage," in *Proc. Int. Symp. Antennas Propag. (ISAP)*, Oct. 2022, pp. 193–194.
- [10] A. L. Amadjikpe, D. Choudhury, C. E. Patterson, B. Lacroix, G. E. Ponchak, and J. Papapolymerou, "Integrated 60-GHz antenna on multilayer organic package with broadside and end-fire radiation," *IEEE Trans. Microw. Theory Techn.*, vol. 61, no. 1, pp. 303–315, Jan. 2013.
- [11] J. Park, I. Jang, B. Seong, and W. Hong, "Differentially-fed, 1-D phased array antenna-on-display featuring wideband and polarization agility for millimeter-wave wireless applications," *IEEE Trans. Antennas Propag.*, vol. 71, no. 9, pp. 7196–7205, Sep. 2023.
- [12] J. Oh, B. Kim, S. Yoon, K. Kim, E. J. Sung, and J. Oh, "High-gain invisible antenna-in-display using non-optical space for 5G smartphones," *IEEE Trans. Antennas Propag.*, vol. 71, no. 2, pp. 1458–1468, Feb. 2023.
- [13] J. Park, S. Y. Lee, J. Kim, D. Park, W. Choi, and W. Hong, "An optically invisible antenna-on-display concept for millimeter-wave 5G cellular devices," *IEEE Trans. Antennas Propag.*, vol. 67, no. 5, pp. 2942–2952, May 2019.
- [14] N. O. Parchin, J. Zhang, R. A. Abd-Alhameed, G. F. Pedersen, and S. Zhang, "A planar dual-polarized phased array with broad bandwidth and quasi-endfire radiation for 5G mobile handsets," *IEEE Trans. Antennas Propag.*, vol. 69, no. 10, pp. 6410–6419, Oct. 2021.
- [15] L. Xue, Q. Tan, K. Cheng, and K. Fan, "A wideband folded dipole antenna with an improved cross-polarization level for millimeter-wave applications," *Appl. Sci.*, vol. 12, no. 21, p. 11291, Nov. 2022.
- [16] H. Yang et al., "Aperture reduction using downward and upward bending arms for dual-polarized quadruple-folded-dipole antennas," *IEEE Antennas Wireless Propag. Lett.*, vol. 22, no. 3, pp. 645–649, Mar. 2023.
- [17] S. Yan, P. J. Soh, and G. A. E. Vandenbosch, "Wearable dual-band magneto-electric dipole antenna for WBAN/WLAN applications," *IEEE Trans. Antennas Propag.*, vol. 63, no. 9, pp. 4165–4169, Sep. 2015.
- [18] C. Chen, "A compact wideband endfire filtering antenna inspired by a uniplanar microstrip antenna," *IEEE Antennas Wireless Propag. Lett.*, vol. 21, no. 4, pp. 853–857, Apr. 2022.
- [19] S. R. Best, "Improving the performance properties of a dipole element closely spaced to a PEC ground plane," *IEEE Antennas Wireless Propag. Lett.*, vol. 3, pp. 359–363, 2004.
- [20] C. Ballesteros, S. Vega, M. C. Santos, and L. Jofre-Roca, "Short asymmetrical inductive dipole antenna for direct matching to high-Q chips," *IEEE Antennas Wireless Propag. Lett.*, vol. 22, no. 1, pp. 149–153, Jan. 2023.
- [21] S. Das, D. J. Sawyer, N. Diamanti, A. P. Annan, and A. K. Iyer, "A strongly miniaturized and inherently matched folded dipole antenna for narrowband applications," *IEEE Trans. Antennas Propag.*, vol. 68, no. 5, pp. 3377–3386, May 2020.
- [22] W. Zhang, Y. Li, K. Wei, and Z. Zhang, "Dual-band decoupling for two back-to-back PIFAs," *IEEE Trans. Antennas Propag.*, vol. 71, no. 3, pp. 2802–2807, Mar. 2023.